HHS Public Access

Author manuscript

Sens Actuators B Chem. Author manuscript; available in PMC 2026 July 16.

Published in final edited form as:

Sens Actuators B Chem. 2026 November 01; 466: . doi:10.1016/j.snb.2026.140282.

Rapid and accessible tumor necrosis factor alpha detection using digital nanoparticle sensors towards point-of-care cytokine monitoring

Maziyar Kalateh Mohammadi[1,2,3,*], **Mohammad Altarfa**[1,2,3,*], **Seyedsina Mirjalili**[1,2,3], **MD Ashif Ikbal**[1,2,3], **Yeji Choi**[1,2,3], **Chao Wang**[1,2,3,**]

[1]School of Electrical, Computer, and Energy Engineering, Arizona State University, Tempe, AZ, US, 85287

[2]Biodesign Center for Molecular Design and Biomimetics, Arizona State University, Tempe, AZ, US, 85287

[3]Center for Photonic Innovation, Arizona State University, Tempe, AZ, USA, 85287

Abstract

Cytokine monitoring is essential for understanding immune response and evaluating therapeutic outcomes in inflammatory and autoimmune diseases. Here, Tumor Necrosis Factor-alpha (TNF-α) is employed as an exemplary cytokine marker to demonstrate a nanoparticle-supported, rapid, electronic detection (NasRED) assay as an one-pot, in-solution sensing platform for cytokine quantification and therapeutic monitoring. Gold nanoparticles (AuNPs) functionalized with TNF Receptor-2 (TNFR2) are designed to react with TNF-α in phosphate-buffered saline (PBS), human pooled serum (HPS), whole blood (WB), cerebrospinal fluid (CSF), and synovial fluid, producing accelerated AuNP precipitation for signal transduction and digitization. The NasRED TNF-α assay demonstrates high sensitivity (1.2 fM), a broad dynamic range of seven orders of magnitude, and a short assay time (~20 min). Importantly, the platform enables analysis of the competitive interactions among TNFR2, TNF-α, and the therapeutic antibody Adalimumab, enabling rapid and multiparametric cytokine assessment. Furthermore, the NasRED assay is explored for detecting TNF-α in the presence of both Adalimumab and anti-drug antibody (ADA), modeling drug resistance scenarios during long-term therapy. This proof of principle study establishes a

Corresponding author: Chao Wang: wangch@asu.edu.
*Equal collaboration

Author contributions

M.K.M. and M.A. designed and performed the experiments. M.K.M. analyzed the data and wrote the manuscript. S.M., M.A.I., and Y.C. contributed to experiment design, PED readout system, and manuscript revision. C.W. conceived the idea, provided the resources, supervised the project, directed experimental design and data interpretation, and co-wrote the manuscript. All authors contributed to discussions and approved the final version.

Declaration of Competing Interest

The authors declare the following competing financial interest(s): C.W. and S.M. are co-founders of REDX Diagnostics, LLC. M.K.M. and C.W. are inventors listed on a patent application relevant to some of the data included in this article. While the underlying technology may be subject to future commercialization, the affiliation did not influence the reported research findings. The remaining authors declare no competing interests.

rapid, digital, and in-solution assay framework for cytokine and therapeutic monitoring in various biofluids and complex competitive environments, paving the way for improved understanding and management of inflammatory, autoimmune, oncological, and neurodegenerative diseases.

Graphical Abstract

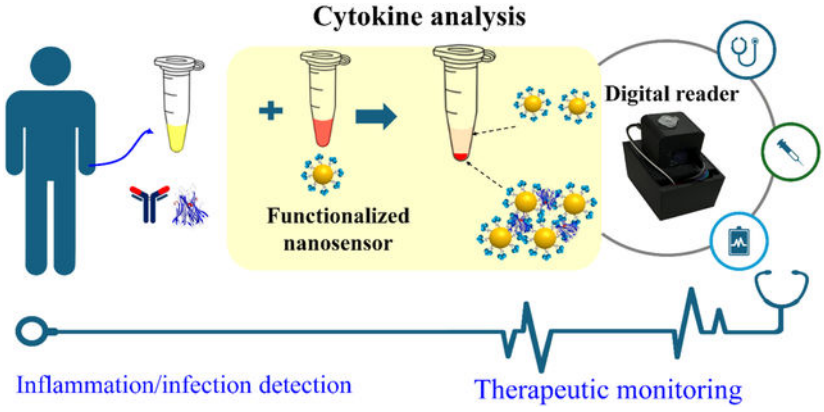

Keywords

Inflammatory disease; Cytokine detection; TNF-alpha; near-patient biosensor; gold nanoparticles (AuNPs); therapeutic monitoring

1. Introduction

The human immune system operates as the body's defense mechanism, safeguarding living organisms from invasion by viruses, bacteria, and parasites [1,2]. Cytokines, small proteins secreted by cells, hold significant biological importance, particularly in cellular signaling[3,4]. Tumor Necrosis Factor-alpha (TNF-α), a pro-inflammatory cytokine produced by macrophages/monocytes, participates in the immune response, plays a role in various physiological events, especially during an inflammatory response, and is directly associated with processes such as fever, apoptosis, sepsis, and myocardial suppression [3,5–7]. However, overexcretion of TNF-α can also contribute to acute inflammation and chronic autoimmune disorders such as Inflammatory bowel disease (IBD) (Crohn's disease [8] and ulcerative colitis [9]), Sepsis [10], and Rheumatoid Arthritis [11]. For instance, roughly over 2.39 million Americans were diagnosed with IBD in 2020, more than 0.7% of the U.S. population [12]. These diseases have negative impacts on the quality of patients' lives, their healthcare consumption behavior, and associated costs [13]. Additionally, cytokine release syndrome can occur during novel cancer immunotherapies as a potentially life-threatening adverse event when large numbers of proinflammatory cytokines (including TNF-α) are released [14,15]. Consequently, measuring the level of TNF-α in biological fluids such as serum, blood, and saliva provides valuable information about the diagnosis, severity, and prognosis of these diseases [3,16].

Currently, treatment with Anti-TNF-α antibodies (Abs, e.g., Adalimumab) is a promising method for managing the progression of various diseases [17,18], including Crohn's

disease[18,19]. However, its efficacy is challenged by the elicitation of immunogenic responses, including production of anti-drug antibodies (ADA) [17,20,21]. Therefore, effective patient treatment and disease management require a personalized analysis that thoroughly considers crucial factors, including immunogenicity potential, treatment safety profiles, and optimal therapy duration. Evaluation of such factors necessitates a facile and accurate measurement tool in clinical decision-making. Given the intricate and dynamic nature of the human immune system, rapid analysis of TNF-α with high accuracy, sensitivity, and throughput is necessary for detecting and monitoring biomarker signatures and their subtle changes [22]. Numerous detection methods have been developed to measure amounts of TNF-α in biofluids (Table 1). Common centralized methods of TNF-α assays, such as enzyme-linked immunosorbent assay (ELISA), radioimmunoassay (RIA), and bioassays, are sensitive but costly, time-consuming, labor-intensive, and instrument-heavy [23,24]. Additionally, a large sample volume is needed to achieve a notable signal-to-noise ratio for detection. Therefore, a persistent need remains for a simple, cost-effective, and sensitive TNF-α test, particularly for point-of-care (POC) applications.

Building on our previously validated nanoparticle-supported rapid electronic detection (NasRED) platform [25], we propose a scenario-specific TNF-α assessment system engineered for clinically relevant immunological conditions, enabling personalized treatment. The assay combines multicomponent biochemical modules with functionalized gold nanoparticle (AuNP) transducers to enable rapid and timely quantification of free TNF-α in complex clinical contexts, including anti-TNF therapy and anti-drug immune responses. This modularity allows the platform to interpret key patient immune states, including cytokine secretion, treatment efficacy, and treatment interference, rather than simply reporting protein levels. Therefore, NasRED presents a generalizable protein-sensing technology with a strong potential for real-time therapeutic monitoring, supporting research and clinical diagnostics across inflammatory, autoimmune, oncological, and neurodegenerative diseases.

2. Experimental section

2.1. Reagents and apparatus

The Biotinylated tumor necrosis factor receptor-2 (TNFR2) (TN2-H82E3), Human TNF-α Protein (GMP-TNAH23), Monoclonal Anti-TNF-α Antibody (16H5) (TNA-AM494), Anti-Drug-Antibody (AY19) (ADB-Y19), Human Interferon Gamma (IFN-γ) (IFG-H4211), Human Interleukin-6 Protein (IL-6) (IL6-H4218), Human Interleukin-10 Protein (IL-10) (IL0-H5218), and Human Arginase-1 Protein (ARG1) (AR1-H5228) were purchased from ACROBiosystem (Newark, DE, USA). Phosphate-buffered saline (PBS) and DNase/RNase-free distilled (DI) water were purchased from Fisher Scientific (Hampton, NH, USA). Human Pooled Serum (HPS) (C817B46), Single donor Human Whole Blood (WB) (IWB1K2E10ML), and Pooled Human Cerebrospinal Fluid (CSF) (IRHUCSF1ML) were purchased from Innovative Research Inc (Novi, MI, USA). Single Human Synovial Fluid (991–42-S-1) was purchased from Medix Biochemica (St. Louis, MO, USA). Bovine serum albumin (BSA) and molecular biology grade glycerol from Sigma-Aldrich (St. Louis, MO,

USA). The streptavidin-functionalized AuNPs were purchased from Cytodiagnostics Inc. (Burlington, ON, Canada) and dispersed in 20% v/v glycerol and 1 wt% BSA buffer.

2.2. Assay modality and design concept

Despite our success in protein detection using NasRED, the mechanical and optical principles of the system remain unchanged in this study. Briefly, NasRED operates through binding-mediated AuNP aggregation resulting from antigen–antibody interactions. Considering the complexity of different scenarios for TNF-α analysis, we design and demonstrate a few different assay formats here, depending on the sample composition. Our in-solution assay employs gold nanoparticles functionalized with TNFR2, membrane proteins that bind specifically to TNF-α [26–28], (AuNPs/TNFR2) (Fig. 1a), as the receptor representing transducers, TNF-α as the antigen, Adalimumab as the therapeutic agent, and ADA as the immunogenicity indicator (Fig. 1b). In the binding assay (Fig. 1c), the TNF-α binding to TNFR2 on functionalized AuNPs leads to the AuNPs clustering. Produced signals are proportional to the TNF-α concentration, which reduces solution color intensity in a naked-eye setup. In the drug efficacy assay (Fig. 1d), the presence of Adalimumab competes with AuNPs/TNFR2 for binding to TNF-α. When sufficient drug molecules are present, they occupy the TNF-α epitopes, preventing AuNPs from clustering. This competitive preservation of free-floating AuNPs maintains their optical extinction properties in solution. Conversely, in the ADA assay (Fig. 1e), ADA binds to Adalimumab and blocks its interaction with TNF-α, allowing free TNF-α to engage with AuNPs/TNFR2 and trigger AuNP aggregation, consequently reducing solution optical extinction. Centrifugation accelerated these interactions by increasing the collision frequency between functionalized AuNPs and their targets in solution. A short (10 min) incubation period, a sufficient time established in our previous work [25], allows aggregate growth within the pellet. Subsequently, vortex agitation-induced turbulent flow resuspended the non-reactive AuNPs fraction, generating the measurable optical extinction signal (Fig. 1f). These extinction changes were quantified using our portable electronic detector (PED), which integrates an LED, photodiode, battery, and signal-stabilizing/processing electronics, similar to our prior works [29,30] (Fig. 1g). Leveraging the assay's biochemical and fluidic modularity, our platform enables rapid detection, suitable for POC use.

2.3 Electronic readout system design

The output signals were digitized using our customized PED, detailed in our previous work [25]. Briefly, it comprised four key components: an LED light source, a photodiode, a microcentrifuge tube chamber, and semiconductor circuits integrated on a printed circuit board (PCB) (Fig. 1h). The tube chamber was 3D-printed using an ABSplus P430 thermoplastic. An 8.6 mm diameter recess was designed to snugly fit a standard 500 μL Labcon microtube. Holes of 2.8 mm diameter were opened on two sides of the microcentrifuge tube chamber to align an LED (597–3311–407NF, Dialight), the upper-level assay liquid, and a photodiode (SFH 2270R, Osram Opto Semiconductors). The LED was powered by two Duracell Optimum AA batteries (3 V) through a serially connected 35 Ω resistor to set the LED operating point. The photodiode was reversely biased by three Duracell Optimum AA batteries (4.5 V) and serially connected to a 7 MΩ load resistor. The photocurrent responding to the intensity of light transmitted through the assay was converted

to voltage through the 7 MΩ load resistor and measured using a portable multimeter (AstroAI AM33D).

2.4. Assay buffer preparation

The assay buffer was prepared by diluting 10×PBS and mixing it with glycerol to increase viscosity [31,32] and BSA to reach a final concentration of 1×PBS, 20% v/v glycerol, and 1 wt% BSA, and stored in a 15 mL conical centrifuge tube at 4 °C. The selected BSA concentration, as reported by the nanoparticle provider (Cytodiagnostics, Inc.), was confirmed to provide sufficient surface passivation and nanoparticle stability.

2.5. Sensing solution preparation

Here, the AuNPs in the assay buffer were functionalized with TNFR2 using a biotin-streptavidin reaction for coating. The lyophilized biotinylated human TNFR2 was reconstituted with 125 μL of sterile DI water to a stock solution of 200 μg/mL (6.97 μM) and diluted to 2 μM using the assay buffer. Then, the streptavidin-coated AuNPs (0.13 nM, 80nm AuNPs, 50 μL) were first mixed with an excessive amount (~ 5 times molar ratio) of biotinylated TNFR2 (2 μM, 20 μL) to achieve a saturated surface coverage. The mixture was then incubated for at least 2 h to ensure complete streptavidin-biotin conjugation. Next, upon addition of 630 μL of the assay buffer, the mixture was purified by centrifugation (accuSpin Micro 17, Thermo Fisher) at 10,000 rounds per minute (rpm) (9600× g) for 10 min following supernatant exchange (630 μL of assay buffer) and repeated twice to remove unbound TNFR2.

2.6. Optimization of sensing solution optical density

After the purification step, precise amounts of the sensing solution were added to six separate tubes, with concentrations ranging from 24 pM to 5 pM, mixed with 100 nM TNF-α solution. As a result of this test, the purified sensing solution was diluted by adding assay buffer to achieve a final AuNPs concentration of 16.25 pM. Concentration was adjusted according to optical density (OD) measurements, as described in detail in our prior studies [25,33].

2.7. TNF-α binding assay

The biological media included PBS, HPS, WB, CSF, and synovial fluid. Among them, PBS, HPS, and CSF were used as purchased without further dilution. Dilution was performed to minimize matrix-induced interference in WB and synovial fluid. Initially, 40 μL of WB and 50 μL of synovial fluid were each mixed with 160 μL and 150 μL of assay buffer, respectively, to prepare 20% and 25% matrices. The lyophilized TNF-α was reconstituted in DI water to prepare a stock solution of 600 μg/mL (32.79 μM). From this stock, 5 μL was diluted individually into 36 μL of biological media (PBS, HPS, 20% WB, CSF, and 25% synovial fluid) to achieve a final concentration of 4 μM. Subsequent serial dilutions were performed using the corresponding biological matrix, with the designated dilutions ranging from 4 μM to 4 fM. Then, 18 μL of the prepared AuNP/TNFR2 solution was mixed with 6 μL of TNF-α solutions at each concentration (100 nM to 1 fM) in microcentrifuge tubes. As a blank negative control (NC), 6 μL of each biological medium without TNF-α was mixed

with the sensing solutions to evaluate the matrix-induced background noise under the same assay conditions. TNF-α sample tubes and NC tubes, each with a total volume of 24 μL, were centrifuged at 3.5 krpm (1180× g) for 5 min. They were then incubated for 10 min, followed by vortexing at 32.5 rounds per second (rps) (1950 rpm) for 5 s.

2.8. TEM imaging preparation

For TEM imaging, 3 μL samples were collected from the bottom of freshly tested tubes (1 pM, 1 fM, and NC) across three independent experiments, dropped onto carbon-coated copper (Cu) grids, and allowed to dry under vacuum to remove residual solvent. The dried grids were analyzed using a TEM/STEM Talos F200i (Thermo Fisher Scientific Inc.) at an accelerating voltage of 200 kV.

2.9. Stability assay

For stability assessment, the AuNPs/TNFR2 solution was stored at 4 °C and tested on days 0, 3, 7, and 14. On each day, 18 μL of AuNPs/TNFR2 was incubated with 6 μL of TNF-α solution to a final concentration of 1 nM, or with 6 μL of assay buffer for the NC. Also, 10 NC samples were prepared on day 0 to check signal consistency. Then the tubes were centrifuged at 1180× g for 5 min, incubated for 10 min, and vortexed for 5 s at 32.5 rps.

2.10. Reproducibility assay

Reproducibility was assessed by performing three consecutive tests. 18 μL of the prepared AuNP/TNFR2 solution was mixed with 6 μL of TNF-α solution at each concentration (100 nM to 1 fM) and NC in microcentrifuge tubes. Then centrifuged at 1180× g for 5 min, incubated for 10 min, and vortexed for 5 s at 32.5 rps.

2.11. Specificity assay

To evaluate the specificity of the sensing probes, additional cytokines, e.g., IFN-γ, IL-6, and IL-10, along with ARG1, a marker for anti-inflammatory macrophages, were chosen as controls. For this objective, IFN-γ, IL-6, IL-10, and ARG1 were spiked and diluted in HPS (final concentration of 100 nM), while TNF-α (1 nM) served as a positive control. Next, 18 μL of the AuNPs/TNFR2 were incubated with 6 μL of each sample in a microcentrifuge tube and centrifuged at 1180× g for 5 min, incubated for 10 min, and vortexed for 5 s at 32.5 rps.

2.12. Drug efficacy assay

The inhibitory effect of Adalimumab on TNF-α was evaluated by mixing three competing components, conceptually similar to our previous work on the SARS-CoV-2 neutralizing antibody test [33]. First, a dilution series of Adalimumab ranging from 4 μM to 4 fM, including a negative sample (PBS with no Adalimumab), was prepared. Then, 6 μL of each dilution was added to 12 μL of AuNPs/TNFR2, followed by the addition of 6 μL of TNF-α. The final concentrations in each tube were 1 μM to 1 fM for Adalimumab and either 10 nM or 1 nM for TNF-α. The OD of each sample was adjusted to approximately 0.5. Then the tubes were centrifuged at 1180× g for 5 min, incubated for 10 min, and vortexed for 5 s at 32.5 rps.

2.13. ADA assay

The impact of ADA on the effectiveness of Adalimumab was determined in a separate experiment. The lyophilized ADA was reconstituted and serially diluted to concentrations ranging from 6 μM to 6 fM. Then, 4 μL of each dilution was added to 12 μL of AuNPs/TNFR2, followed by the addition of 4 μL of TNF-α and 4 μL of Adalimumab. The final concentrations in each tube were 1 μM to 1 fM for ADA, 50 nM for Adalimumab, and either 10 nM or 1 nM for TNF-α. The OD of each sample was adjusted to approximately 0.5. Then the tubes were centrifuged at 1180× g for 5 min, incubated for 10 min, and vortexed for 5 s at 32.5 rps.

2.14. Competitive binding assay

To evaluate the extent of competition TNF-α between Adalimumab and ADA, another set of sensors was needed. The lyophilized biotinylated ADA was reconstituted in DI water to a final concentration of 600 μg/mL and diluted to 2 μM. Then, 50 μL of streptavidin-coated AuNPs were added to 20 μL of diluted biotinylated ADA and mixed. The mixture was then incubated for at least 2 h to ensure complete streptavidin-biotin conjugation, and the purification step was performed as described for the preparation of AuNPs/TNFR2 sensors. For the assay, 18 μL of the functionalized gold nanoparticles with ADA (AuNPs/ADA) was added to 6 μL of the dilution series (1 μM −1 fM final concentration) of TNF-α and Adalimumab individually. The OD was adjusted to 0.5, and the tubes were centrifuged at 1180× g for 5 min, incubated for 10 min, and vortexed for 5 s at 32.5 rps.

2.15. Data analysis and LOD calculation

The tubes were measured using our PED. For data analysis, a background signal calibration was performed. Each tube was filled with assay buffer, and 15 measurements were collected by rotating tubes in 5 different orientations to eliminate the tube variability and averaged to establish the background electronic readout (E_{ref}) as a reference:

$$E_{ref} = \frac{\sum_i \left(E_{ref,i}\right)}{15} (i = 1 \text{ to } 15) \tag{1}$$

The same tubes were then used to hold the AuNP sensing solution, during which 15 measurements were performed, and the electronic signals for each TNF-α concentration ($E_{test}(C)$) were averaged as follows:

$$E_{test}(C) = \frac{\sum_i \left(E_{test,i}(C)\right)}{15} (i = 1 \text{ to } 15) \tag{2}$$

which C denotes the analyte concentration. Therefore, the tube signal ($S_{PED}(C)$) was normalized as:

$$S_{PED}(C) = \frac{E_{ref} - E_{test}(c)}{E_{ref}} \tag{3}$$

from 1 to 0, e.g., 1 representing no aggregation from a blank sample (no target) and 0 indicating all AuNPs precipitated at a high target concentration. The error of the measurement is the standard deviation (σ) of the 15 normalized signals as follows:

$$\sigma(C) = \sqrt{\frac{\sum_i \left(S_{PED,\,i}(C) - S_{PED}(C)\right)^2}{15 - 1}} (i = 1 \text{ to } 15) \tag{4}$$

The signals were plotted and fitted using biphasic dose-response fitting and the sigmoidal equation in Origin 2024b software (OriginLab, USA), employing the orthogonal distance regression algorithm to account for data and error weights in the fitting calculations. The biphasic signal pattern is triggered by active fluidic manipulation rather than solely biochemical saturation or multivalency, which is related to the exponential decay function of the solution [25,34]. The fitting equation is:

$$S_{PED,\,BD}(C) = S_L + (S_H - S_L)\left[\frac{p}{1 + 10^{(log x01 - log C)h_1}} + \frac{1 - p}{1 + 10^{(log x02 - log C)h_2}}\right] \tag{5}$$

where $S_{PED,BD}$ represents the standard biphasic dose-response fitting measured from S_{PED}, S_L and S_H correspond to the minimum and maximum signal values, x_{01} and x_{02} are the half-maximal effective concentrations (EC_{50}-1 and EC_{50}-2), h_1 and h_2 are the Hill slopes for the first and second response phases, and p defines the curve steepness. Furthermore, the limit of detection (LoD) and the limit of quantification (LoQ) were calculated such that the measured signal distinguished from the reference signal by 3 and 10 times the standard deviation of the reference, respectively, following:

$$S_{LOD} = S_{NC} - 3 \times (\sigma_{NC}) \tag{6}$$

$$S_{LOQ} = S_{NC} - 10 \times (\sigma_{NC}) \tag{7}$$

The S_{LoD} and S_{LoQ} were then plotted against the corresponding target concentrations to determine the LoD and LoQ in fitted plots.

The relative standard deviation (RSD) for the targeted samples is calculated as:

$$RSD(\%) = \frac{\sigma(C)}{Mean} \times 100\,\% \tag{8}$$

2.16. Spectroscopy measurement

For measuring the optical extinction, 5 μL of the tubes' supernatants (100 nM to 1 fM and NC) was collected and loaded in a PDMS plate. The assay buffer was used as a reference, and optical extinction was measured with a laboratory spectrometer (iHR-320, Horiba Instruments Inc.). To achieve optimal contrast, the focal plane was adjusted to the well plate surface. Three spots were selected within each well (one at the center and two near the edges) to account for possible inhomogeneity in AuNP distribution. Transmitted light from each spot was collected using a 50× objective lens (NA = 0.8), and transmission spectra were recorded over the 350–700 nm range with an integration time of 0.01 s, averaging 64 measurements per spot. The average sample values were subtracted from the background noise (T), and the same was done for the assay buffer (T_b). The optical extinction (ΔExtinction) was normalized:

$$\Delta Extinction(C) = \frac{T_b - T(C)}{T_b} \tag{9}$$

from 1 to 0, e.g., 1 representing no aggregation from the blank sample (no target) and 0 indicating all AuNPs precipitated at a high target concentration.

3. Results and discussion

NasRED was designed as a one-pot assay to detect the target protein interactions in solution by simply mixing the bodily fluids with functionalized AuNPs. The mixing, reaction, and readout were all completed in the same tube without any washing, labeling, or fluorescent imaging, thus greatly reducing the complexity of the operation.

3.1. Impact of sensing protocol on performance

NasRED operates with active fluidic forces rather than relying on passive diffusion, as in traditional methods such as ELISA or SPR, which was found critical to the signal transduction in our previous studies [25,35]. Centrifugation and vortex agitation can significantly modulate the distribution of reagents and AuNPs in the buffer solutions, thereby strongly affecting the optimal conditions for achieving the best sensitivity and specificity in a given biological medium. On the one hand, sufficiently strong and long centrifugation plays several important roles in promoting rapid and highly sensitive antibody-antigen reactions. First, it serves to spin the AuNPs and reagents at a high speed for active mixing. Second, centrifugation also acts to shorten the assay time by elevating the collision rate of reactants, which is mainly limited by the sedimentation speed of AuNPs. With centrifugation, the precipitation length of AuNPs significantly drops from a few millimeters (here the height of the colloid liquid, dependent on the buffer volume and

the tube size) to the micrometer scale, therefore eliminating hours-long precipitation time that is otherwise required and significantly speeding up signal transduction and readout [25,30,35]. Third, centrifugation also localizes AuNPs and their clusters with a greatly boosted concentration (estimated by 45000 times volume reduction and concentration increasing) at the bottom of the reaction tube [25], thus moving the dynamic equilibrium of the antigen-antibody reaction to favor AuNP cluster formation even at a low reagent concentration in the tube [30].

On the other hand, sufficient vortex agitation is needed to resuspend monomeric AuNPs that are not incorporated into clusters, allowing them to return to a free-floating state, in order to ensure high specificity; i.e., the NCs should revert to their initial states. Still, the vortex force cannot be excessively high to break the AuNP clusters “glued” together, which would negatively affect sensitivity. Therefore, the speed and time of vortex agitation need to be adjusted in conjunction with the centrifugation conditions.

Ideally, a large signal contrast is desired for maximizing the sensitivity, and a large dynamic range, i.e., from <10 fM to 1 μM, is useful to address clinical relevance and sample heterogeneity. Interestingly, these desired metrics were satisfied within a relatively broad range of centrifugation conditions, i.e., from 600 g to 1950 g and from 1 to 8 min (Fig. 2a–b). Optimal centrifugal forces were required to maximize sensitivity, and excessively high centrifugal speeds and times could form tight AuNP aggregates, which became harder to break under vortex agitation and were therefore avoided in our protocols. Further, vortex conditions, such as time and agitative force, directly affected the clusters’ integrity (Fig. 2c–d). For example, agitative force lower than 1750 rpm (29 rps) did not resuspend the NC, while too strong agitation (above 2400 rpm, 40 rps) led to full cluster dispersion despite a high 1nM target TNF-α concentration (1nM). Taking all the above into consideration, we chose a standard processing condition for all tests in this work, i.e., centrifugation for 5 min at 1,180g (3.5 krpm), incubation for 10 min, and vortexing for 5 s at 32.5 rps. All other parameters were constant for each stage, and only one variable was changed at a time.

Furthermore, the final probe concentration was optimized to ensure assay sensitivity (Fig. S1a). Among the six tested conditions, a probe concentration of 16.25 pM, which corresponded to an initial OD of approximately 0.5, produced the highest signal (Fig. S1b–c) and was therefore selected as the standard concentration for subsequent assays (Fig. S1d).

3.2. TNF-α binding assay

To prove the concept of TNF-α detection for diagnosis purposes, we applied AuNPs/TNFR2 sensor in various biological fluids (Fig. 3). First, TNF-α was spiked in PBS (Fig. 3a), showing concentration-dependent aggregation, while no aggregation was seen in the NC (Fig. 3b). The assay achieved a LoD of 1.2 fM (0.022 pg/mL) and a LoQ of 40 fM (0.73 pg/mL), demonstrating the feasibility of highly sensitive cytokine detection through the NasRED platform. Additionally, a direct ELISA test was performed as a comparison (Fig. S2a) by coating TNF-α and adding a dilution series of TNFR2, yielding a LoD of 8.2 pM (0.23 ng/mL) and LoQ of 25.6 pM (0.73 ng/mL) (Fig. S2b). The monotonic decrease in the free-probe signal with increasing TNF-α confirms that the data are consistent with the aggregation mechanism, as modeled for the binding assay (Fig. S3b, supplementary

material Section 3). In comparison to relevant demonstrations (Table 1), NasRED achieved a significantly lower LoD, with a rapid assay time (20 min) and minimal sample input (only 6 μL). For example, a reported microfluidic electrochemical immuno-chip [36] reached an LOD of 4100 pg/mL with an assay time of 142 min, a long processing time, and a minimum working volume of 100 μL, while the fluorescent microsphere immunoassay ELISA [37] required 3 h and 50 μL of sample to achieve an LoD of 41 pg/mL, and required specialized instrumentation. Novel electrochemical platforms, such as skyscraper [38] biosensors (LoD 44.5 pg/mL, 45 min) or G-PEDOT:PSS electrodes [39] (LoD 5.97 pg/mL, 20 min, 22 μL) have limitations in either detection sensitivity, sample volume, or dependence on electrochemical readout systems and multistep procedures. Collectively, these comparisons underscore NasRED's unique capabilities in POC applications.

3.3. Evaluation of sensor performance in complex biofluids and cross-cytokine specificity

Further, we evaluated the performance of AuNPs/TNFR2 sensors for detecting TNF-α in HPS, CSF, and synovial fluid (joint fluid) to assess the sensor's versatility and effectiveness in more clinically relevant settings. To conduct the experiment, we prepared TNF-α of different concentrations (1 μM to 1 fM in buffer or biological fluids) and NC samples, and further diluted them in 100% HPS, 100% CSF, 20% whole blood, and 25% synovial fluid (Fig. 3a–d). Clearly, the AuNPs/TNFR2 sensors successfully detected TNF-α across all tested biological media (Fig. 3d), with a femtomolar-level sensitivity. More specifically, the LoD values were 6.6 fM in HPS, 1.7 fM in CSF, 3.5 fM in 20% whole blood, and 3.1 fM in 25% synovial fluid (Table S1), which were derived from the corresponding data of biphasic dose-response fitting equations (Table S2), comparable with the single molecular array (Simoa) assay that achieved an LoD of 0.013 pg/mL (0.72 fM) in a 25% serum-like matrix [40]. Also, the LoQ values were calculated as 37 fM in HPS, 71 pM in CSF, 60nM in 20% whole blood, and 533 pM in 25% synovial fluid (Table S1). The LoD values in HPS were ~6-fold worse compared to those in PBS, attributable to the presence of serum proteins and increased viscosity [25,33,35], which biomechanically influenced sensor performance, yet the LoQ values were quite similar. In comparison, tests in CSF were comparable to those in PBS and HPS in terms of LoD values, indicating only moderate biofouling and optical interference. Further, TNF-α testing in synovial fluid was complicated by the high viscosity, which could introduce additional mechanofluidic resistance and adversely affect the sensitivity. Tests in whole blood were further challenged by overlapping optical absorption of hemoglobin with AuNP extinction and biofouling effects, producing nM LoQ, consistent with our previous studies [25,33]. Given the modular design of the NasRED system, further optimization, e.g., using high-affinity and cobinding antibodies [25], will likely enhance sensitivity and shorten assay time for POC use.

To visualize nanoparticle clustering at the micro- and nanoscale, TEM images (Fig. 3e, Fig. S4a–c) captured AuNP morphology at two TNF-α concentrations and the NC, with increased nanoparticle aggregation observed at higher TNF-α levels compared to the well-dispersed NC sample. EDS analysis of the NC sample (Fig. S4d) confirmed the presence of Au, buffer components, and proteins bound to the AuNPs. Also, statistical analysis of TEM images (Fig. S5) revealed clear concentration-dependent clustering behavior. At 1 pM TNF-

α (Fig. S5a–b), AuNPs exhibit a broad distribution of cluster sizes, including a significant fraction of large aggregates, whereas at 1 fM (Fig. S5c–d), clustering shifts toward smaller populations with fewer large aggregates. In contrast, the NC (Fig. S5e–f) predominantly consists of small clusters with minimal aggregation, indicating effective nanoparticle dispersion. Particle size analysis confirms a relatively uniform AuNP diameter (Fig. S5g). Overall, these results demonstrate a concentration-dependent increase in nanoparticle aggregation with increasing TNF-α levels (Fig. S5h). Furthermore, spectroscopic analysis using a HORIBA spectrometer evaluated TNF-α-induced AuNP aggregation by measuring the supernatant from vortexed tubes, attributed to free-floating AuNPs. Transmission intensity spectra of samples (10 nM to 1 fM and NC) showed a concentration-dependent optical response (Fig. S6a). Changes in extinction values (Fig. 3f) revealed distinct optical differences across concentrations. Notably, analysis at 550 nm (Fig. S6b) enabled clear differentiation between TNF-α concentrations ranging from 10 nM to 1 fM and the NC. The selection of 550 nm is attributed to its proximity to the AuNP localized surface plasmon resonance (LSPR) band [41,42], where aggregation-induced changes produce pronounced optical variations.

The stability of the nanosensors was evaluated over a 14-day period. As a result, nanoparticles retained ~97% of their initial signal, indicating their stability, while the response to 1 nM TNF-α retained ~89% of its initial value (Fig. 3g). AuNPs/TNFR2 signal consistency also had a variation below 5% over 10 testing tubes (Fig. S7a). Furthermore, reproducibility measurements at TNF-α concentrations ranging from 100 nM to 1 fM yielded RSD below 4% for all concentrations, except 1 nM (7%) (Fig. S7b), demonstrating good measurement consistency of the sensing platform.

Specificity is particularly critical in inflammatory diagnostics, where multiple cytokines can be simultaneously elevated. Various cytokines play central roles in immune regulation and are frequently used as biomarkers in diseases such as rheumatoid arthritis, sepsis [10], tuberculosis [43], autoimmune disorders [5], and cytokine release syndrome (CRS) [14,15]. For example, IL-6 is a key mediator of inflammatory responses, while IFN-γ, produced by T cells and natural killer cells, is essential for host defense against intracellular pathogens and is implicated in autoimmunity [44,45]. IL-10 inhibits the production of proinflammatory cytokines (such as IL-6, TNF-α, and IL-12) and chemokines, while ARG1 is a cytosolic enzyme that catalyzes the hydrolysis of L-arginine into urea and L-ornithine to reduce inflammatory activity, and it is a well-characterized marker for anti-inflammatory (M2) macrophage polarization and inflammatory resolution [46–51]. CRS associated with adoptive T-cell therapies consistently presents elevated levels of IL-6, IFN-γ, and TNF-α along with immunoregulatory mediators such as IL-10 and ARG1, which are associated with suppressive myeloid cell activity. Therefore, IL-6, IL-10, IFN-γ, and ARG1 were selected as representative cytokines and tested in HPS at 100 nM, 100 times higher than TNF-α (1 nM). These proteins did not elicit an appreciable NasRED response, with their corresponding signals indistinguishable from the NC (Fig. 3g). These results demonstrated that the AuNP sensors could maintain the specificity within a complex matrix without serious nonspecific adsorption or biofouling. Such performance is desirable in clinical use for the accurate quantification of TNF-α and other cytokines while reducing false positives from interfering inflammatory markers.

3.4. Protein interaction evaluation

To understand the complex protein binding dynamics that affect NasRED performance, we further engineered the sensor platform to analyze the complex interactions between TNF-α and multiple antibodies, including Adalimumab and ADA (Fig. 4). To accomplish that, ADA was functionalized on AuNPs and used to bind free-floating Adalimumab (Fig. 4a–c) and TNF-α (Fig. 4d–e). To examine ADA–Adalimumab interactions, Adalimumab was serially diluted across seven orders of magnitude (1 μM to 1 fM, plus NC) and mixed with AuNPs/ADA sensors in PBS (Fig. 4a). As visualized (Fig. 4b), the addition of Adalimumab induced pronounced AuNP aggregation across a wide concentration range, resulting in a clear gradation in colorimetric response. Quantitative analysis of the extinction signal (Fig. 4c) yielded a bi-sigmoidal response with a phase transition within a concentration window between ~1 pM and 100 pM (dashed lines, Fig. 4c), characteristic of complex fluidic dynamic interactions involving AuNPs under the NasRED sensing process [25]. The observed LoD of ~1 pM underscored the high sensitivity of our platform, comparable with that achieved by ELISA (LoD of 4.4 pM, or 0.65 ng/mL; LoQ of 15.3 pM, or 2.3 ng/mL) (Fig. S2c–d). In contrast, no visible aggregation was observed when AuNPs/ADA probes were mixed with TNF-α across the same concentration range (Fig. 4d–f), yielding extinction signals nearly identical to the NC and confirming minimal nonspecific cross-reactivity between ADA and TNF-α.

The observed strong ADA binding to Adalimumab but minimal interaction with TNF-α allowed us to introduce ADA in our multi-protein analytical system to study the molecular competition between cytokines and antibodies (Figs. 1d–e). As ADA binds Adalimumab strongly with a low-picomolar LoD, it significantly affects drug–target interaction with TNF-α.

3.5. Drug efficacy and ADA assay

Next, we evaluated how ADA and Adalimumab influence the competitive balance between TNF-α and Au/TNFR2, simulating anti-TNF-α therapy. First, a three-component protein competition assay was designed, consisting of serially diluted Adalimumab (1 μM to 1 fM, plus NC), AuNPs/TNFR2 probes (at 16.25 pM), and free TNF-α antigen (at 1 nM and 10 nM) (Fig. 5a). The two TNF-α concentrations were selected to simulate different disease severity, and specifically designed at these nM range, because the TNF-α binding to AuNPs/TNFR2 sensors would produce visually distinguishable colorimetric changes, favorable for optimal signal transduction. The introduced Adalimumab would compete with TNFR2 for TNF-α binding, similar to our previously reported competitive sensing strategies [33], effectively neutralizing TNF-α at high concentrations and thereby preventing TNF-α binding to TNFR2. Therefore, high levels of Adalimumab dose would keep the AuNPs/TNFR2 probes dispersed, producing uniform red solution color with a high optical extinction (Fig. 5b). Conversely, low dose (for example below 1 nM) drug was insufficient to completely block TNF-α binding to TNFR2 on the AuNPs, and thus AuNP aggregation proceeded, producing a signal correlated with the TNF-α concentration (Fig. 5c). Notably, a large signal modulation (~100–0.5 nM Adalimumab, dashed region, Fig. 5c) marked the transition from high drug efficacy (full TNF-α neutralization) to drug deficiency. For cross-reference, ELISA was performed by testing a dilution series of Adalimumab against

TNF-α (Fig. S2e), showing a LoD of 3.1 pM (0.17 ng/mL) and a LoQ of 11.5 pM (0.63 ng/mL) (Fig. S2f), validating the accuracy of the tests. Competitive-binding mechanism was validated following Michaelis–Menten kinetics and the kernel principle [52–54], in which increasing adalimumab at a fixed TNF-α lowers the signal as modeled in the supplementary material (Fig. S3c, supplementary material section 3).

Next, ADA was further introduced, at varying concentrations, to the three-component mixture to examine its impact on anti-TNF-α antibody response (Fig. 5d). In this design, aggregation of AuNPs/TNFR2 probes is modulated by the amount of free TNF-α, which in turn depends on the available Adalimumab not sequestered by ADA. Clinically, circulating Adalimumab levels in treated patients generally exceed 4.5 μg/mL and are most often maintained between 8–12 μg/mL [55–57]. Accordingly, Adalimumab was chosen at 50 nM (~8 μg/mL) in our assay for two representative TNF-α levels, i.e., 1 nM (moderate disease, Fig. 5e top image and Fig. 5f red line) and 10 nM (simulating severe disease, Fig. 5e bottom image and Fig. 5f black line). As visualized in optical tube images and further quantitatively measured by PED readouts, Adalimumab failed to neutralize all TNF-α when ADA was present at 100 nM and higher concentrations, leading to AuNP aggregation and diminished AuNP extinction signal. In comparison, at lower ADA concentrations (e.g. <100 pM), AuNPs were less aggregated, because Adalimumab remained largely available to effectively neutralize TNF-α, suppressing TNF-α-mediated AuNP precipitation. This observation also aligns with the molecular kinetics in Michaelis–Menten and kernel principles [52–54], which is reflected in our experimental modeling for signal prediction (Fig. S3d, supplementary material section 3). Notably, in our approach the presence of ADA was measured indirectly via a competitive binding reaction with anti-TNF-α antibodies, supporting a comprehensive analysis of TNF-α levels in complex biological fluids. Collectively, these findings served to establish the feasibility of a simple and rapid in-solution assay capable of evaluating drug efficacy and ADA interference in TNF-α detection, demonstrating the platform's potential as a clinically relevant tool for monitoring therapeutic antibody performance and immunogenicity.

3.6. Artificial serum test

To assess the assay's translational performance in a clinically relevant environment, we next evaluated TNF-α detection in artificial patient serum prepared from 100% HPS. For each experiment, AuNPs/TNFR2 probes were mixed with TNF-α (600 nM, 60 nM, and 6 nM), Adalimumab (300 nM, 30 nM, 3 nM, and 30 pM), and ADA (600 nM and 30 pM) in a total reaction volume of 24 μL, i.e., 12 μL AuNP probe solution and 4 μL for each of the three protein solutions diluted in 100% HPS. The mixture was briefly vortexed at 2000 rpm for 5 s to ensure homogeneity. Notably, the protein concentration in the mixture was thus diluted to 1/6 of the supplied concentration.

As an example, ADA was supplied at 60 nM and mixed with TNF-α and Adalimumab at varied concentrations, keeping a final ADA concentration of 10 nM (Fig. 6a). In this configuration, the assay exhibited a clear competitive response, with the aggregation of AuNPs/TNFR2 probes highly dependent on both TNF-α and Adalimumab concentrations, similar to our previous discussions (Fig. 5a). At high TNF-α concentrations (final

concentration 50 nM after mixing, Fig. 6a top row), the AuNP probes fully aggregated regardless of the Adalimumab concentration to produce a clear solution, suggesting ineffective Adalimumab for highly severe case. At moderate TNF-α levels (final concentration 5 nM, Fig. 6a middle row), higher Adalimumab concentration would neutralize more TNF-α, thus suppressing AuNP aggregation, while a lower amount of Adalimumab (e.g., <1 nM) was insufficient for neutralization. In contrast, at low TNF-α levels (final concentration 0.5 nM, Fig. 6a bottom row), no aggregation occurred across the full tested Adalimumab concentration range (1 nM to 100 nM in the mixture), demonstrating complete neutralization of TNF-α in the presence of ADA. Further quantitative analysis of the NasRED PED signals revealed a clear trend of decreasing AuNP extinction with increasing Adalimumab at given TNF-α concentrations (Fig. 6b).

In a second test scenario, the ADA concentration was set tenfold higher at a final concentration of 100 nM, while the TNF-α and Adalimumab concentrations varied (Fig. 6c). Under these conditions, Adalimumab neutralization of TNF-α was strongly impaired across the tested concentrations, leading to more AuNP aggregation at higher TNF-α concentrations. Quantitative PED signal analysis (Fig. 6d) further illustrated the complexity of TNF-α detection, consistent with the lower ADA scenario (Fig. 6b). As the TNF-α concentration decreased from high to low (50 to 0.5 nM), AuNP aggregation was correspondingly reduced. Consistent with 10 nM ADA results, PED signals decreased when Adalimumab concentration was reduced at given TNF-α concentrations. As a control, samples without TNF-α were included as a reference, showing no AuNP aggregation even in the presence of high (10 nM or 100 nM) Adalimumab and ADA, confirming the specificity of our assay. Noticeably, the PED signal in detecting TNF-α was much more sensitive to Adalimumab at higher ADA concentrations. For example, with TNF-α at 0.5 nM, the difference between PED signals at 100 nM Adalimumab (S_1, red dashed line) and 10 nM (S_2, green dashed line), i.e., $\delta S = S_1 - S_2$, was 0.06 and 0.24 when ADA was supplied at 10 nM (Fig. 6b) and 100 nM (Fig. 6d), respectively. At higher TNF-α concentration, both the PED signal and the signal difference became much smaller. For instance, at 5 nM TNF-α, δS in 10 nM Adalimumab was 0.04, while for 100 nM ADA was around 0.16. Additionally, the signal between 10 nM and 100 nM ADA at the same concentrations of TNF-α and Adalimumab showed a significant drop (from 1 to 0.78, red dashed lines and 0.93 to 0.54, green dashed lines) (Table 2). Taken together, these findings underscore the reliability and specificity of our assay for detecting TNF-α. While this study is not clinically focused, a formal clinical decision strategy will be more appropriate in future studies involving patient specimens for specific diseases. To this end, we propose a hypothetical clinical workflow integrating NasRED-based TNF-α detection with diagnostic evaluation and treatment decision-making (Fig. S8), which serves as a conceptual framework for guiding patient management.

4. Conclusions and outlook

This work establishes NasRED as a new, one-pot diagnostic platform for quantitative assessment of TNF-α and drug–target competition in clinically relevant matrices. Using TNFR2-functionalized AuNPs and a palm-sized electronic reader, the assay detects TNF-α at a LoD of 1.2 fM in PBS with a 7-log dynamic range and a total turnaround

of ~20–25 min from mix to readout, while requiring only 6 μL of sample. NasRED outperformed conventional TNF-α assays in sensitivity, assay speed, and sample economy (benchmarked in Table 1). Further, NasRED maintained high analytical performance in various biological fluids despite background interference molecules, including 100% HPS (LoD 6.6 fM), CSF (LoD 1.7 fM), 20% whole blood (LoD 3.5 fM), and 25% synovial fluid (LoD 3.1 fM), and demonstrated high specificity against other cytokines and mediators at high concentrations (IL-6, IL-10, ARG1, and IFN-γ at 100 nM) without cross-reactivity. Uniquely, our NasRED platform is capable of analyzing competition between TNFR2, TNF-α, therapeutic Adalimumab (anti-TNF-α antibody), and ADA, underscoring its potential as a practical tool for monitoring therapeutic efficacy and ADA interference across different stages of treatment. Our findings demonstrate that the NasRED platform functioned well in complex serum matrices, delivering rapid (~25 min), portable, and sensitive analysis of TNF-α in the picomolar range and suggesting its use as a promising tool to track therapy effectiveness and ADA interference in clinical samples. Collectively, NasRED features single-tube workflow, short assay time, femtomolar level sensitivity, multifunctional analysis of complex interfering antibodies, applicability in different biofluids, and precise, digital, and portable readout. This technological advancement addresses a clinically important need with diagnostic and therapeutic implications across inflammatory and autoimmune diseases and can have broadened use in oncologic and neurodegenerative disease management.

While this work establishes the design and analytical performance of the NasRED cytokine assay, future efforts will focus on clinical validation using well-characterized patient specimens. Assay robustness, selectivity, and reliability are expected to vary across disease contexts, including inflammatory disorders (e.g., Crohn’s disease, ulcerative colitis, rheumatoid arthritis), sepsis, and cytokine release syndrome associated with cancer immunotherapy. Accordingly, the sensor design, assay workflow, and statistical analysis methods will require further optimization to account for differences in sample handling (e.g., storage time and temperature) and patient heterogeneity. Addressing these challenges will require close collaboration with clinical partners, and insights from clinical datasets will guide the translation of NasRED into practical diagnostic and therapeutic monitoring workflows. From a technological perspective, the current workflow involves manual vortexing steps that may introduce user-dependent variability. Future development of a miniaturized, automated platform capable of integrating sample processing (e.g., centrifugation and mixing), signal acquisition, and data analysis will improve assay reproducibility and usability. In addition, integration of electronic readout circuitry with embedded control and data-processing modules will enable streamlined system operation and facilitate deployment in near-patient or POC settings.

Supplementary Material

Refer to Web version on PubMed Central for supplementary material.

Acknowledgements

We would like to acknowledge Dr. Howard A. Young from the National Cancer Institute for the supportive discussions, and Manuel Roldan Gutierrez from Eyring Materials Center, ASU, for the assistance in TEM Imaging. We also thank Nimarpreet Bamrah and Sean McClure for their collaborations. We acknowledge partial support

from the National Science Foundation (grant no. 1847324) and the National Institutes of Health (grant nos. R21AI169098, R21AI186134, and DP2GM149552).

Biographies

Maziyar Kalateh Mohammadi, Ph.D. student, with the group since Aug 2022

Email: mkalateh@asu.edu

I received my bachelor's degree in Chemical Engineering in 2017 and my master's degree in Biotechnology-Chemical Engineering in 2021 at University of Tehran. Currently, I'm a PhD candidate in Electrical Engineering at Arizona State University under the supervision of Dr. Chao Wang. My research interests are nanofabrication and nanobiosensing. Besides that, I also love listening to music, playing video games and traveling.

Mohammad (Momo) Altarfa, with the group from Aug 2022 to June 2023

Email: maltarfa@asu.edu

I received my bachelor's degree in Electrical Engineering with an emphasis in Electrical Engineering at Northern Arizona University in 2020. My dissertations research interests are nanobody synthesis and bimolecular detection. Besides that, I enjoy watching soccer.

Seyedsina Mirjalili, doctorate received 2025, with the group since Aug 2022 to Dec 2025

Email: smirjali@asu.edu

I received a B.A.Sc. in Cellular & Molecular Biology (Microbiology field) in 2016 (SBU, Iran) and an M.Sc. Dual Degree in Nanobiotechnology (TMU, Iran) and Bio-Entrepreneurship (CBS, Denmark) in 2020. During the past years, I have worked on and developed a passion for innovative Nano-biosensors for Diagnostics. I graduated with a PhD in Electrical Engineering from Arizona State University, and I am currently a postdoctoral researcher at York University, Canada. Apart from conducting experiments and SME businesses, I am also a horse rider, piano player, swimmer, and a gigantic fan of MCU.

Md Ashif Ikbal, with the group from Sep 2017 to Aug 2022

Email: mikbal@asu.edu

I received my bachelor's degree in Chemical Engineering from Bangladesh University of Engineering and Technology. I obtained my Master's degree from Yeungnam University, South Korea. My research interests are nanomaterials synthesis and fabrication for bio sensing application. Besides research, I like to watch movies an sports, listen to music and travel photography. Ashif graduated in 2022 and joined Intel.

Yeji Choi, Ph.D. student, with the group since Aug 2022

Email: ychoi128@asu.edu

I received my bachelor's and Master's degree in Information and Communication Engineering From Pukyong National University Of Engineering, South Korea, in 2019 and 2021, respectively. Currently, I'm a PhD candidate in Electrical Engineering at Arizona State University under the supervision of Dr. Chao Wang. My research interests include biosensors, nanomaterials, and analog circuit design, etc. Besides research, I also love hiking, traveling, and working out in a gym.

Chao Wang, Ph.D.

Associate Professor

School of Electrical, Computer & Energy Engineering, Ira A. Fulton Schools of Engineering

Biodesign Center for Molecular Design & Biomimetics

Graduate faculty of Physics, Material Science & Engineering, and Biomedical Engineering

Arizona State University

ERC 539, 551 E. Tyler Mall, Tempe, AZ 85281

Cell: 609-375-7798

Office (zoom call): 480-965-2056

Email: wangch@asu.edu

Lab Web: https://nanobio.engineering.asu.edu/

Associate Professor; Office: ERC 539; Email: wangch@asu.edu; Phone: 480-965-2056

Education

- **Ph.D., Dept. Electrical Engineering, Princeton University**, January 2012
- **M.A., Dept. Electrical Engineering, Princeton University**, September 2008
- **M. S., Institute of Microelectronics, Tsinghua University**, July 2006
- **B.E., Dept. Electronic Engineering, Tsinghua University**, July, 2003

Academic Experience

- **Aug 2022-Present** Associate Professor, Arizona State University
- **Feb 2016-July 2022** Assistant Professor, Arizona State University
- **Jan 2015–Jan 2016** Research Assistant Professor, Arizona State University
- **2012–2014** Postdoctoral research scientist, IBM T.J. Watson research center
- **2012** Postdoctoral research associate, Princeton University

References

[1]. Janeway CA, Medzhitov R, Innate immune recognition, Annu. Rev. Immunol 20 (2002) 197–216. 10.1146/annurev.immunol.20.083001.084359. [PubMed: 11861602]

[2]. Iwasaki A, Medzhitov R, Control of adaptive immunity by the innate immune system, Nat. Immunol 16 (2015) 343–353. 10.1038/ni.3123. [PubMed: 25789684]

[3]. Liu C, Chu D, Kalantar-Zadeh K, George J, Young HA, Liu G, Cytokines: From Clinical Significance to Quantification, Advanced Science 8 (2021). 10.1002/advs.202004433.

[4]. Liu G, Zhang K, Nadort A, Hutchinson MR, Goldys EM, Sensitive Cytokine Assay Based on Optical Fiber Allowing Localized and Spatially Resolved Detection of Interleukin-6, ACS Sens. 2 (2017) 218–226. 10.1021/acssensors.6b00619. [PubMed: 28723139]

[5]. Jang DI, Lee AH, Shin HY, Song HR, Park JH, Kang TB, Lee SR, Yang SH, The role of tumor necrosis factor alpha (Tnf-α) in autoimmune disease and current tnf-α inhibitors in therapeutics, Int. J. Mol. Sci 22 (2021) 1–16. 10.3390/ijms22052719.

[6]. Sedger LM, McDermott MF, TNF and TNF-receptors: From mediators of cell death and inflammation to therapeutic giants - past, present and future, Cytokine Growth Factor Rev. 25 (2014) 453–472. 10.1016/j.cytogfr.2014.07.016. [PubMed: 25169849]

[7]. Chaudhry H, Zhou J, Zhong Y, Ali MM, Mcguire F, Nagarkatti PS, Nagarkatti M, Role of Cytokines as a Double-edged Sword in Sepsis, In Vivo (Brooklyn). 27 (2013) 669–684. http://iv.iiarjournals.org/content/27/6/669.abstract (accessed May 25, 2026).

[8]. Mirza MSS, Khan M, Rahman MS, Nadeem A, Anugu GR, Masmoum MD, Hameed Z, Khawar MH, Mansoor M, Comparative Efficacy of Anti-tumor Necrosis Factor (TNF) Therapy in Inducing and Maintaining Remission from Crohn's Disease: A Systematic Review and Meta-analysis, J. Adv. Med. Med. Res 36 (2024) 105–121. 10.9734/jammr/2024/v36i95561.

[9]. Florholmen J, Goll R, Johnsen KM, Intensified anti-TNF treatment downregulates the phenotype in ulcerative colitis: a 13-year prospective follow-up study, Frontiers in Gastroenterology 2 (2023). 10.3389/fgstr.2023.1304944.

[10]. Gharamti AA, Samara O, Monzon A, Montalbano G, Scherger S, DeSanto K, Chastain DB, Sillau S, Montoya JG, Franco-Paredes C, Henao-Martínez AF, Shapiro L, Proinflammatory cytokines levels in sepsis and healthy volunteers, and tumor necrosis factor-alpha associated sepsis mortality: A systematic review and meta-analysis, Cytokine 158 (2022). 10.1016/j.cyto.2022.156006.

[11]. Arora J, Mendelson AA, Fox-Robichaud A, Sepsis: network pathophysiology and implications for early diagnosis, Am. J. Physiol. Regul. Integr. Comp. Physiol 324 (2023) R613–R624. 10.1152/AJPREGU.00003.2023. [PubMed: 36878489]

[12]. Lewis JD, Parlett LE, Jonsson Funk ML, Brensinger C, Pate V, Wu Q, Dawwas GK, Weiss A, Constant BD, McCauley M, Haynes K, Yang JY, Schaubel DE, Hurtado-Lorenzo A, Kappelman MD, Incidence, Prevalence, and Racial and Ethnic Distribution of Inflammatory Bowel Disease in the United States, Gastroenterology 165 (2023) 1197–1205.e2. 10.1053/j.gastro.2023.07.003. [PubMed: 37481117]

[13]. Aliu A, Bosch DHCA, Keszthelyi D, Rezazadeh Ardabili A, Colombel JF, Sawyer R, Törnblom H, Hart A, Jonkers DMAE, Pierik MJ, Mujagic Z, Review article: A practical approach to persistent gastrointestinal symptoms in inflammatory bowel disease in remission, Aliment. Pharmacol. Ther (2024). 10.1111/apt.17988.

[14]. Morris EC, Neelapu SS, Giavridis T, Sadelain M, Cytokine release syndrome and associated neurotoxicity in cancer immunotherapy, Nat. Rev. Immunol 22 (2022) 85–96. 10.1038/s41577-021-00547-6. [PubMed: 34002066]

[15]. Lee DW, Gardner R, Porter DL, Louis CU, Ahmed N, Jensen M, Grupp SA, Mackall CL, Current concepts in the diagnosis and management of cytokine release syndrome, Blood 124 (2014) 188–195. 10.1182/blood-2014-05-552729. [PubMed: 24876563]

[16]. Hirten RP, Lin KC, Whang J, Shahub S, Helmus D, Muthukumar S, Sands BE, Prasad S, Longitudinal assessment of sweat-based TNF-alpha in inflammatory bowel disease using a wearable device, Sci. Rep 14 (2024). 10.1038/s41598-024-53522-1.

[17]. Ogrič M, Terčelj M, Praprotnik S, Tomšič M, Božič B, Sodin-Semrl S, Čučnik S, Detection of adalimumab and anti-adalimumab antibodies in patients with rheumatoid arthritis: a comprehensive overview of methodology pitfalls and benefits, Immunol. Res 65 (2017) 172–185. 10.1007/s12026-016-8824-8. [PubMed: 27421721]

[18]. Asgharpour A, Cheng J, Bickston SJ, Adalimumab treatment in crohn's disease: An overview of long-term efficacy and safety in light of the extend trial, Clin. Exp. Gastroenterol 6 (2013) 153–160. 10.2147/CEG.S35163. [PubMed: 24039442]

[19]. D'Haens GR, Van Deventer S, 25 years of anti-TNF treatment for inflammatory bowel disease: Lessons from the past and a look to the future, Gut 70 (2021) 1396–1405. 10.1136/gutjnl-2019-320022. [PubMed: 33431575]

[20]. Vermeire S, Gils A, Accossato P, Lula S, Marren A, Immunogenicity of biologics in inflammatory bowel disease, Therap. Adv. Gastroenterol 11 (2018). 10.1177/1756283X17750355.

[21]. van Loo G, Bertrand MJM, Death by TNF: a road to inflammation, Nat. Rev. Immunol 23 (2023) 289–303. 10.1038/s41577-022-00792-3. [PubMed: 36380021]

[22]. Chen P, Chung MT, McHugh W, Nidetz R, Li Y, Fu J, Cornell TT, Shanley TP, Kurabayashi K, Multiplex serum cytokine immunoassay using nanoplasmonic biosensor microarrays, ACS Nano 9 (2015) 4173–4181. 10.1021/acsnano.5b00396. [PubMed: 25790830]

[23]. Leng SX, McElhaney JE, Walston JD, Xie D, Fedarko NS, Kuchel GA, ELISA and Multiplex Technologies for Cytokine Measurement in Inflammation and Aging Research, The Journals of Gerontology: Series A 63 (2008) 879–884. 10.1093/gerona/63.8.879.

[24]. Petrovas C, Daskas SM, Lianidou ES, Determination of Tumor Necrosis Factor-(TNF-) in Serum by a Highly Sensitive Enzyme Amplified Lanthanide Luminescence Immunoassay, Clin. Biochem 32 (1999) 241–247. 10.1016/S0009-9120(99)00004-1. [PubMed: 10463815]

[25]. Choi Y, Mirjalili S, Ikbal MA, McClure S, Mohammadi MK, Clemens S, Solano J, Heggland J, Zhang T, Zuo J, Wang C, Nanoparticle-Supported, Rapid, and Electronic Detection of SARS-CoV-2 Antibodies and Antigens at the Subfemtomolar Level, ACS Nano 19 (2025) 30509–30524. 10.1021/acsnano.5c12083. [PubMed: 40788688]

[26]. Rauert H, Wicovsky A, Müller N, Siegmund D, Spindler V, Waschke J, Kneitz C, Wajant H, Membrane Tumor Necrosis Factor (TNF) induces p100 processing via TNF receptor-2 (TNFR2), Journal of Biological Chemistry 285 (2010) 7394–7404. 10.1074/jbc.M109.037341. [PubMed: 20038584]

[27]. Tschopp J, Schneider P, Bodmer J-L, The molecular architecture of the TNF superfamily, Trends Biochem. Sci 27 (2002) 19–26. 10.1016/S0968-0004(01)01995-8. [PubMed: 11796220]

[28]. Takahashi H, Yoshimatsu G, Faustman DL, The Roles of TNFR2 Signaling in Cancer Cells and the Tumor Microenvironment and the Potency of TNFR2 Targeted Therapy, Cells 11 (2022). 10.3390/cells11121952.

[29]. Ikbal MDA, Kang S, Chen X, Gu L, Wang C, Picomolar-Level Sensing of Cannabidiol by Metal Nanoparticles Functionalized with Chemically Induced Dimerization Binders, ACS Sens. 8 (2023) 4696–4706. 10.1021/acssensors.3c01758. [PubMed: 38084058]

[30]. Chen X, Kang S, Ikbal MA, Zhao Z, Pan Y, Zuo J, Gu L, Wang C, Synthetic nanobody-functionalized nanoparticles for accelerated development of rapid, accessible detection of viral antigens, Biosens. Bioelectron 202 (2022). 10.1016/j.bios.2022.113971.

[31]. Zhang L, Zhang X, Zhang P, Zhang Z, Liu S, Han B, Efficient emulsifying properties of glycerol-based surfactant, Colloids Surf. A Physicochem. Eng. Asp 553 (2018) 225–229. 10.1016/j.colsurfa.2018.05.055.

[32]. Brown JR, Madsen MD, Ateş A, Islam R, Agbo B, Nikoo KK, Lattimer BY, Long TE, Revealing foam stability for cationic and zwitterionic triethylsilyl-containing surfactants, Physics of Fluids 35 (2023). 10.1063/5.0152198.

[33]. Mirjalili S, Ikbal MA, Hou CW, Mohammadi MK, Choi Y, Kelbauskas L, VanBlargan LA, Hogue BG, Murugan V, Diamond MS, Wang C, Nanoparticle-supported, rapid, digital quantification of neutralizing antibodies against SARS-CoV-2 variants, Biosens. Bioelectron 285 (2025). 10.1016/j.bios.2025.117549.

[34]. Midelet J, El-Sagheer AH, Brown T, Kanaras AG, Werts MHV, The Sedimentation of Colloidal Nanoparticles in Solution and Its Study Using Quantitative Digital Photography, Particle and Particle Systems Characterization 34 (2017). 10.1002/ppsc.201700095.

[35]. Mohammadi MK, Mirjalili S, Ikbal MA, Xie H, Wang C, Rapid and Sensitive Detection of Thrombospondin-2 Using Nanoparticle Sensors for Cancer Screening and Prognosis, Micromachines (Basel). 16 (2025). 10.3390/mi16030354.

[36]. Eletxigerra U, Martinez-Perdiguero J, Merino S, Disposable microfluidic immune-biochip for rapid electrochemical detection of tumor necrosis factor alpha biomarker, Sens. Actuators B Chem 221 (2015) 1406–1411. 10.1016/j.snb.2015.08.026.

[37]. Hall SA, Stucke D, Morrone B, Lebelt D, Zanella AJ, Simultaneous detection and quantification of six equine cytokines in plasma using a fluorescent microsphere immunoassay (FMIA), MethodsX 2 (2015) 241–248. 10.1016/j.mex.2015.04.002. [PubMed: 26150994]

[38]. Hussain KK, Hopkins R, Yeoman MS, Patel BA, 3D printed skyscraper electrochemical biosensor for the detection of tumour necrosis factor alpha (TNFα) in faeces, Sens. Actuators B Chem 410 (2024). 10.1016/j.snb.2024.135694.

[39]. Rahman MA, Pal RK, Islam N, Freeman R, Berthiaume F, Mazzeo A, Ashraf A, A Facile Graphene Conductive Polymer Paper Based Biosensor for Dopamine, TNF-α, and IL-6 Detection, Sensors 23 (2023). 10.3390/s23198115.

[40]. Wu D, Milutinovic MD, Walt DR, Single molecule array (Simoa) assay with optimal antibody pairs for cytokine detection in human serum samples, Analyst 140 (2015) 6277–6282. 10.1039/c5an01238d. [PubMed: 26270328]

[41]. Takahata R, Tsukuda T, Ultrathin gold nanowires and nanorods, Chem. Lett 48 (2019) 906–915. 10.1246/cl.190313.

[42]. Joplin A, Chang WS, Link S, Imaging and Spectroscopy of Single Metal Nanostructure Absorption, Langmuir 34 (2018) 3775–3786. 10.1021/acs.langmuir.7b03154. [PubMed: 29149571]

[43]. Khelghati F, Rahmanian M, Eghbal E, Seghatoleslami ZS, Goudarzi M, Keramatinia A, Ong CW, Goletti D, D'Ambrosio L, Centis R, Nasiri MJ, Migliori GB, Risk of tuberculosis disease in patients receiving TNF-α antagonist therapy: A meta-analysis of randomized controlled trials, New Microbes New Infect. 62 (2024). 10.1016/j.nmni.2024.101533.

[44]. Lüder CGK, IFNs in host defence and parasite immune evasion during Toxoplasma gondii infections, Front. Immunol 15 (2024). 10.3389/fimmu.2024.1356216.

[45]. McLoughlin RM, Witowski J, Robson RL, Wilkinson TS, Hurst SM, Williams AS, Williams JD, Rose-John S, Jones SA, Topley N, Interplay between IFN-γ and IL-6 signaling governs neutrophil trafficking and apoptosis during acute inflammation, Journal of Clinical Investigation 112 (2003) 598–607. 10.1172/JCI17129. [PubMed: 12925700]

[46]. Carlini V, Noonan DM, Abdalalem E, Goletti D, Sansone C, Calabrone L, Albini A, The multifaceted nature of IL-10: regulation, role in immunological homeostasis and its relevance to cancer, COVID-19 and post-COVID conditions, Front. Immunol 14 (2023). 10.3389/fimmu.2023.1161067.

[47]. Greenhalgh AD, Passos dos Santos R, Zarruk JG, Salmon CK, Kroner A, David S, Arginase-1 is expressed exclusively by infiltrating myeloid cells in CNS injury and disease, Brain Behav. Immun 56 (2016) 61–67. 10.1016/j.bbi.2016.04.013. [PubMed: 27126514]

[48]. Pesce JT, Ramalingam TR, Mentink-Kane MM, Wilson MS, Kasmi KCE, Smith AM, Thompson RW, Cheever AW, Murray PJ, Wynn TA, Arginase-1-expressing macrophages suppress Th2 cytokine-driven inflammation and fibrosis, PLoS Pathog. 5 (2009). 10.1371/journal.ppat.1000371.

[49]. Rojas JM, Avia M, Martín V, Sevilla N, IL-10: A multifunctional cytokine in viral infections, J. Immunol. Res 2017 (2017). 10.1155/2017/6104054.

[50]. Li Z, Wang L, Ren Y, Huang Y, Liu W, Lv Z, Qian L, Yu Y, Xiong Y, Arginase: shedding light on the mechanisms and opportunities in cardiovascular diseases, Cell Death Discov. 8 (2022). 10.1038/s41420-022-01200-4.

[51]. Iyer S, Cheng G, Role of Interleukin 10 Transcriptional Regulation in Inflammation and Autoimmune Disease, Crit. Rev. Immunol 32 (2012) 23–63. 10.1615/CritRevImmunol.v32.i1.30. [PubMed: 22428854]

[52]. Shi G, Shen X, Ren H, Rao Y, Weng S, Tang X, Kernel principal component analysis and differential non-linear feature extraction of pesticide residues on fruit surface based on surface-enhanced Raman spectroscopy, Front. Plant Sci 13 (2022). 10.3389/fpls.2022.956778.

[53]. Choi B, Rempala GA, Kim JK, Beyond the Michaelis-Menten equation: Accurate and efficient estimation of enzyme kinetic parameters, Sci. Rep 7 (2017). 10.1038/s41598-017-17072-z.

[54]. Cornish-Bowden A, One hundred years of Michaelis–Menten kinetics, Perspect. Sci. (Neth) 4 (2015) 3–9. 10.1016/j.pisc.2014.12.002.

[55]. Dehoorne JL, Groth H, Carlé E, De Schrijver I, Sys C, Delbeke P, Kreps EO, Renson T, Bonroy C, Defining a therapeutic range for adalimumab serum concentrations in the management of pediatric noninfectious uveitis, a step towards personalized treatment, Pediatric Rheumatology 21 (2023). 10.1186/s12969-023-00928-2.

[56]. Plevris N, Lyons M, Jenkinson PW, Chuah CS, Merchant LM, Pattenden RJ, Watson EF, Ho GT, Noble CL, Shand AG, Din S, Arnott ID, Jones GR, Lees CW, Higher Adalimumab Drug Levels during Maintenance Therapy for Crohn's Disease Are Associated with Biologic Remission, Inflamm. Bowel Dis 25 (2019) 1036–1043. 10.1093/ibd/izy320. [PubMed: 30335139]

[57]. Zittan E, Kabakchiev B, Milgrom R, Nguyen GC, Croitoru K, Steinhart AH, Silverberg MS, Higher adalimumab drug levels are associated with mucosal healing in patients with Crohn's disease, J. Crohns Colitis 10 (2016) 510–515. 10.1093/ecco-jcc/jjw014. [PubMed: 26783345]

[58]. Nie Q, Zhang B, Li R, Yang Y, Ren J, Qiu L, Lu Y, Zhu L, Shen H, Liu Y, You R, Ultra-sensitive detection of tumor necrosis factor alpha based on silver-coated gold core shell and magnetically separated recognition of SERS aptamer sensors, Microchimica Acta 191 (2024). 10.1007/s00604-023-06049-7.

[59]. Cao H, Liu J, Wei D, Liu B, Hu Y, Liu J, Wan S, Wu T, He XD, Jiang J, Xu H, Farrell G, Wu Q, Ultrahigh sensitivity fiber laser integrated biosensor for TNF-α detection in human blood sample, Sens. Actuators B Chem 422 (2025). 10.1016/j.snb.2024.136561.

[60]. Borg KN, Jaffiol R, Ho YP, Zeng S, Enhanced biosensing of tumor necrosis facftor-alpha based on aptamer-functionalized surface plasmon resonance substrate and Goos-Hänchen shift, Analyst 149 (2024) 3017–3025. 10.1039/d4an00194j. [PubMed: 38606503]

[61]. Qi M, Zhang Y, Cao C, Zhang M, Liu S, Liu G, Decoration of Reduced Graphene Oxide Nanosheets with Aryldiazonium Salts and Gold Nanoparticles toward a Label-Free Amperometric Immunosensor for Detecting Cytokine Tumor Necrosis Factor-α in Live Cells, Anal. Chem 88 (2016) 9614–9621. 10.1021/acs.analchem.6b02353. [PubMed: 27600768]

Highlights

- One-pot, in-solution cytokine assay with no surfaces, washes, or instrumentation
- Femtomolar LoD (1.2–6.6 fM) across 5 complex biological matrices with broad dynamic range
- Rapid 20-minute workflow outperforming ELISA in speed and simplicity
- Quantifies TNF-α in real world cytokine surge, therapy, and immune interference scenarios

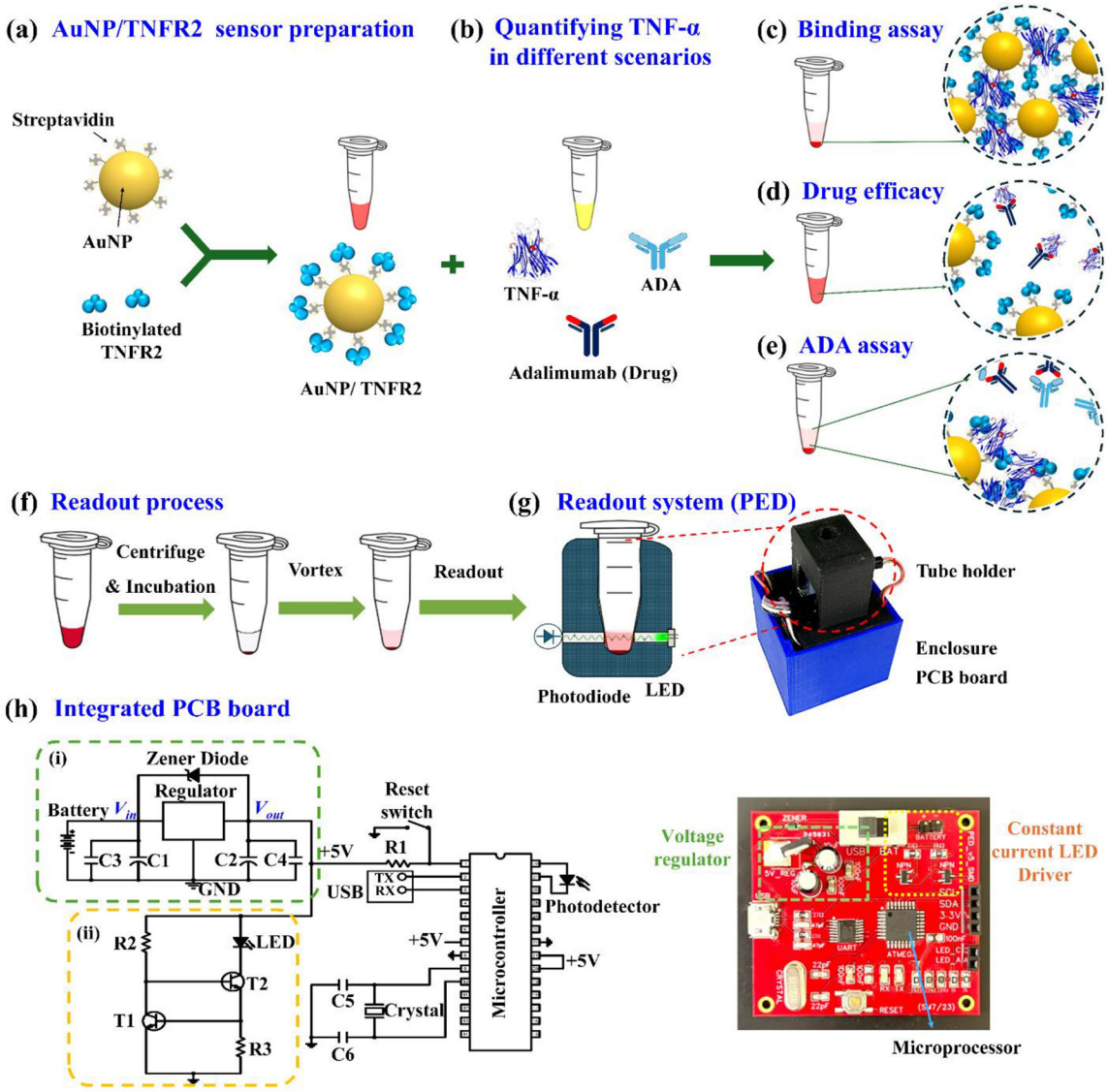

Figure 1:

Schematic of assay design for therapeutic monitoring of TNF-α. (a) AuNP/TNFR2 probes are produced by functionalizing 80 nm streptavidin gold nanoparticles with biotinylated TNFR2. (b) Probes will then be mixed with the sample containing TNF-α and/or Adalimumab and/or ADA (c). A hypothetical diagnosis and prognosis scenario for TNF-α antigen detection (binding test) for disease diagnosis. (d) Detection in a hypothetical on-treatment scenario where anti-TNF-α antibody is present (Drug efficacy test). (e) Detection in a hypothetical scenario where both anti-TNF-α and induced ADA are present in the testing sample (ADA assay). (f) Schematics of the assay process involving Centrifugation, agitation, and signal readout. (g) Optical transmission signal collection of supernatant of the microcentrifuge tube, and using a PED device for converting them to electronic signals. (h) Schematic of the PCB including a voltage regulator, constant-current LED driver, and microcontroller for signal processing and communication (USB, Wi-Fi, or Bluetooth), and the optical image of the PCB used for signal processing.

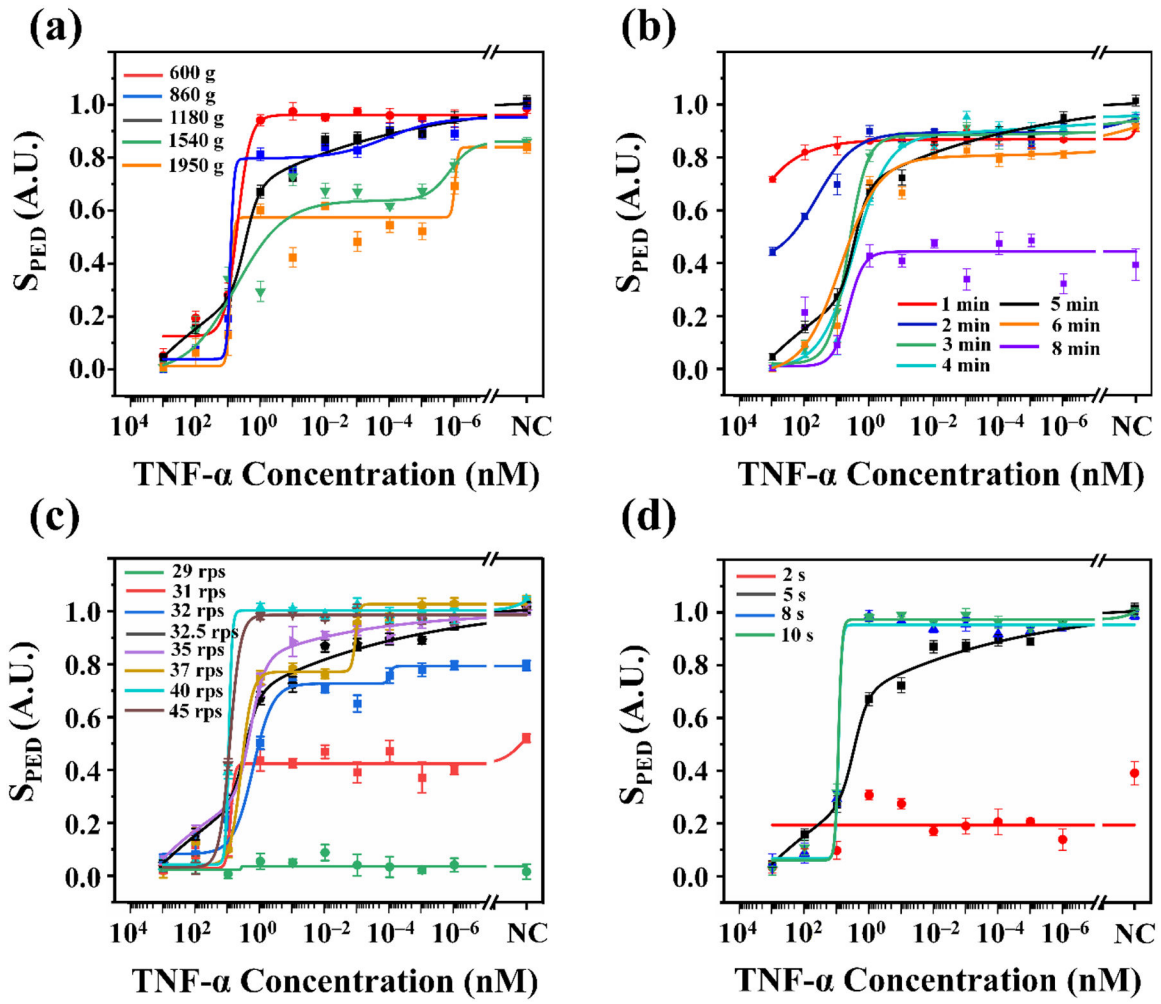

Figure 2:

Engineering process optimization to enhance TNF-α antigen sensing. (a-d) The PED readout signal S_{PED} plotted as a function of TNF-α concentration, with (a) the centrifugal force from 600 to 1950 gravity for 5 min while keeping the vortex condition as 32.5 rps, 5 s, (b) centrifugation time from 1 min to 8 min, (c) different vortexing agitation speed conditions from 29 rps to 45 rps, and (d) vortexing time from 2 s to 10 s. Centrifugation causes AuNP cluster formation, while vortex agitation releases loose AuNPs back into the solution. The error bars correspond to the standard deviation observed across these measurements (n=15).

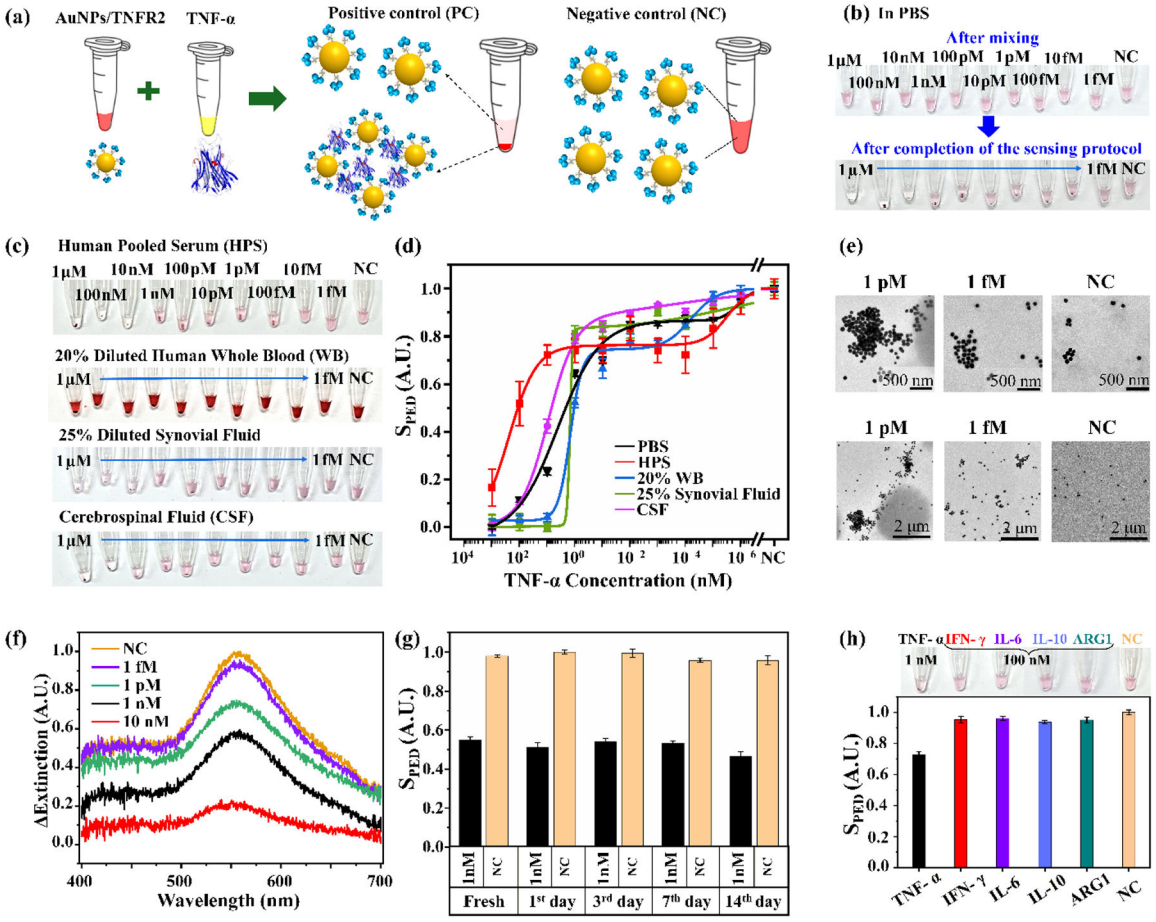

Figure 3:

Demonstrated binding assay to detect TNF-α spiked in PBS. (a) Schematic of TNF-α detection assay with positive and negative sample differentiation, where the presence of TNF-α leads to the formation of AuNP clusters. (b) Optical images of the test tubes holding AuNP sensing buffer mixed with target TNF-α molecules: 'top' after mixing and 'bottom' after the sensing procedure (centrifugation, incubation, and vortex agitation). (c) Visual images of tube arrays for TNF-α detection in HPS, 20% diluted WB, CSF, and 25% diluted synovial fluid using AuNPs/TNFR2 sensors with different concentrations of TNF-α ranging from 1 μM to 1 fM and NC. NC= Biofluid only, where no AuNP precipitates formed. (d) Normalized PED signals with different concentrations of TNF-α plotted in the biofluids, with LoD of 1.2 fM (0.022 pg/mL), 6.6 fM (0.12 pg/mL), 3.5 fM (0.064 pg/mL), 1.7 fM (0.031 pg/mL), and 3.1 fM (3.1 pg/mL) in PBS, HPS, 20% WB, 25% synovial fluid, and CSF, respectively. Error bars indicated σ across PED replicate readouts (n=15). (e) TEM images of AuNPs at two TNF-α concentrations and NC, shown at 500 nm and 2 μm scale bars. (f) ΔExtinction profiles of AuNP supernatants at varying TNF-α concentrations (10 nM, 1 nM, 1 pM, 1 fM, and NC), showing concentration-dependent optical changes associated with nanoparticle sedimentation. (g) Stability test over 14 days (1 nM and NC) (h) Specificity assay, visual image, and plot in TNF-α antigen (1 nM) sensing comparison with IFN-γ (100 nM), IL-6 (100 nM), IL-10 (100nM), ARG1 (100nM), and NC in HPS solution. The tube containing TNF-α showed higher transparency and a differentiable PED

signal even at a lower concentration (1 nM). Error bars indicated σ across PED replicate readouts (n=15)

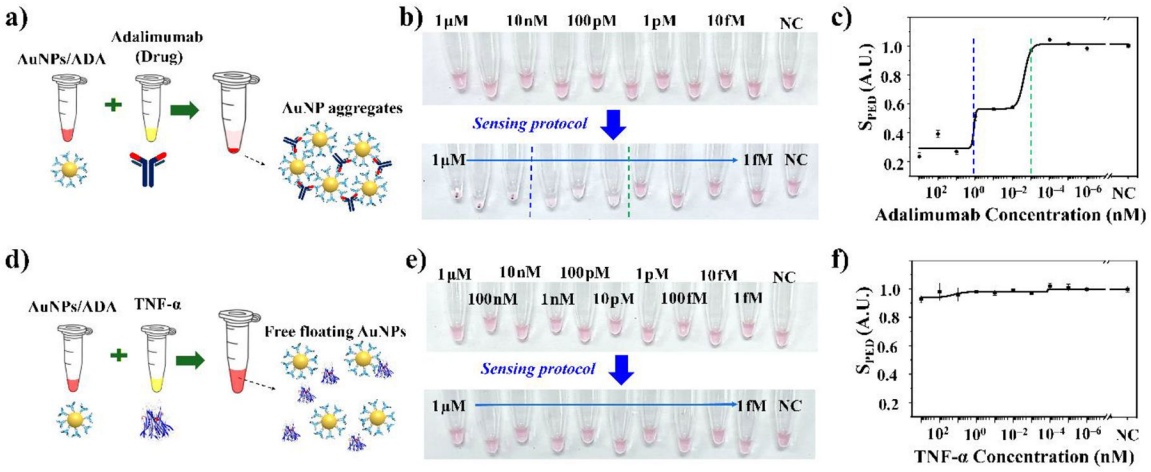

Figure 4:

Evaluation of ADA affinity for Adalimumab and TNF-α. (a) Schematic of AuNPs/ADA mixing with adalimumab to form AuNP clusters after NasRED protocol is performed. (b) Optical images of tubes containing AuNPs/ADA mixed with varying Adalimumab concentrations: 'top' after mixing and 'bottom' after the sensing procedure (centrifugation, incubation, and vortex agitation). (c) Normalized PED signals for Adalimumab binding to Au/ADA in PBS. Dash lines represent a bi-sigmoidal response with a phase transition. (d) Schematic of AuNPs/ADA mixing with TNF-α to evaluate their affinity towards each other, which leads to free-floating AuNPs and TNF-α. (e) Optical images of tubes containing AuNPs/ADA mixed with varying TNF-α concentrations: 'top' after mixing and 'bottom' after the sensing procedure. (f) Normalized PED signals for detecting TNF-α using AuNP/ADA sensors. No specific bindings observed. The error bars correspond to the σ observed across these measurements (n=15).

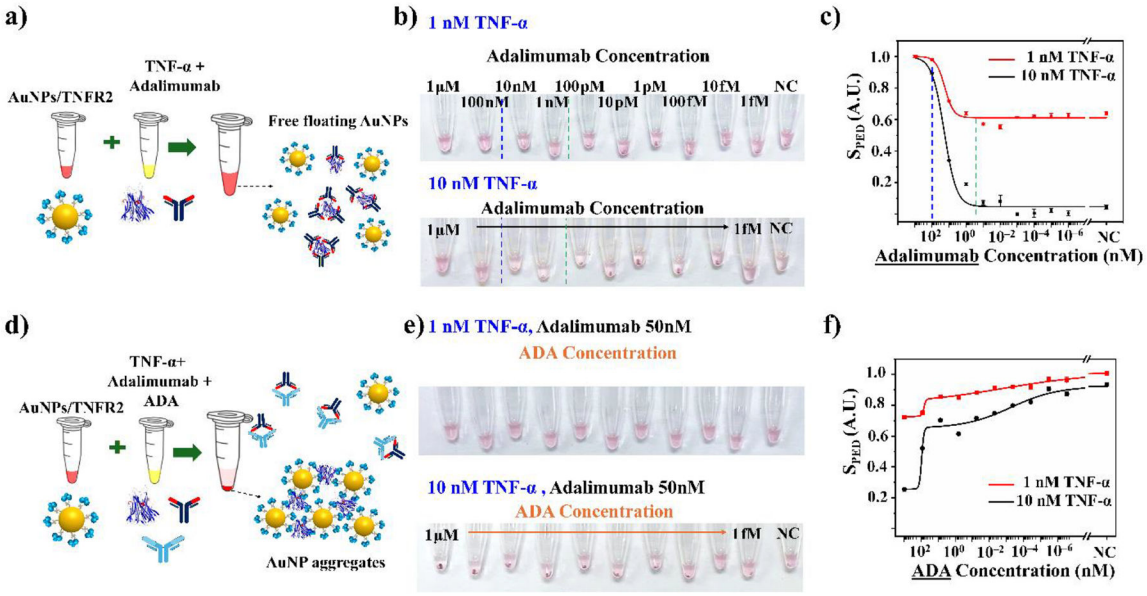

Figure 5:

Demonstrated assays in TNF-α antigen sensing in the presence of Adalimumab (drug) and ADA. (a) Schematic of drug efficacy assay, in which AuNPs/TNFR2 probes are mixed with TNF-α and Adalimumab. After sensing protocol, Adalimumab will inhibit TNF-α, and AuNP probes will be floating. (b) Optical images of drug efficacy after sensing protocol for two TNF-α conditions (1 nM, 10 nM) and Adalimumab, ranging from 1 μM to 1 fM, and NC. NC=no Adalimumab. Top: 1 nM TNF-α; bottom: 10 nM TNF-α. (c) Normalized PED signals to detect TNF-α using AuNPs/TNFR2 probes in the presence of varying concentrations of Adalimumab at 1 nM and 10 nM of TNF-α. (d) Schematic of the ADA test, in which AuNPs/TNFR2 probes are mixed with TNF-α, Adalimumab, and ADA. After sensing protocol, ADA will neutralize Adalimumab and excess TNF-α, and probes will form AuNP clusters. (e) Optical images of ADA test after sensing protocol for two TNF-α conditions (1 nM, 10 nM) and ADA, ranging from 1 μM to 1 fM, and NC in the presence of 50 nM Adalimumab. NC=no ADA. Top: 1 nM TNF-α; bottom: 10 nM TNF-α. (f) Normalized PED signals to detect TNF-α using AuNPs/TNFR2 probes in the presence of varying concentrations of ADA at 1 nM and 10 nM of TNF-α with 50 nM Adalimumab. Data are presented as mean ± σ (n=15).

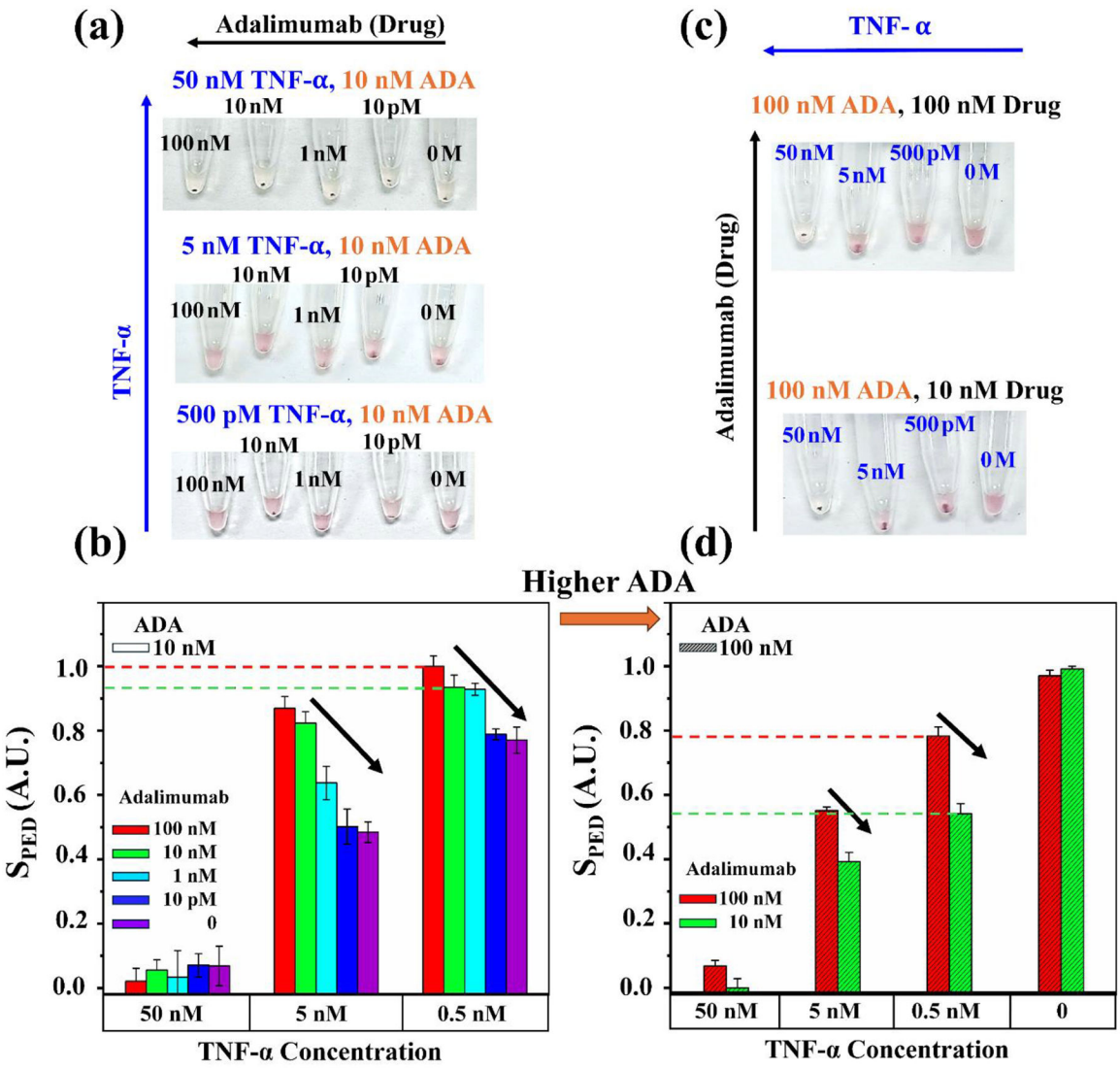

Figure 6:

Demonstrated assays in TNF-α antigen sensing in spiked serum samples using AuNPs/TNFR2 nanosensors. (a) Visual images of tube arrays for TNF-α detection in HPS using AuNPs/TNFR2 with different concentrations of Antibody (100 nM −0 M) with variation of TNF-α (50 nM, 5 nM, 500 pM) and with 10nM ADA (b) Normalized PED signal plotted in aggregate signals using TNF-α as the only variable in 10 nM ADA. Red and green dashed lines highlight the signal change by decreasing Adalimumab from 100 nM to 10 nM (c) 100nM ADA with different concentrations of TNF-α (50 nM – 0 M) with variable Adalimumab concentration (100 nM and 10 nM). The arrows show the effect of Adalimumab on the aggregation of nanosensors. (d) Normalized PED signal plotted in aggregate signals using TNF-α as the only variable in 100 nM ADA, demonstrating the impact of a higher concentration of ADA. The arrows show the effect of Adalimumab on the aggregation of nanosensors. Red and green dashed lines highlight the signal change by decreasing Adalimumab from 100 nM to 10 nM. Data are presented as mean ± σ (n=15).

Table 1.

Comparison of TNF-α detection of some biosensors using different techniques.

Detection method	Linear range (pg/mL)	Medium	LOD (pg/mL)	Assay time	Minimum working volume	Readout method	Ref
Surface-enhanced Raman scattering (SERS) magnetic patch sandwich immunoassay	10^{-3}– 10^{4}	PBS	0.00437	120 min	10 μL	Raman Spectrometer	[58]
skyscraper electrochemical biosensor	160 – 1820	Feces	44.5	45 min	-	Electrochemical voltametric immunoassay	[38]
Microfluidic electrochemical immuno-biochip	0– 5×10^{4}	PBS	4100	142 min	100 μL	Electrochemical immunoassay	[36]
tapered single mode - quad-core –single mode fiber structure biosensor	10– 10^{4}	PBS	10	30 min	1 mL	Spectrometer	[59]
surface plasmon resonance (SPR)	10^{-4}– 10^{6}	PBS	0.05	20 min	-	Spectrometer	[60]
G-PEDOT:PSS	5– 5×10^{4}	PBS	5.97	20 min	22 μL	EIS	[39]
Fluorescent microsphere immunoassay ELISA	41– 10^{4}	PBS	41	3 h	50 μL	Fluorescence spectrometer	[37]
label-free electrochemical immunosensor	10– 150	PBS	0.1	20 min	-	Electrochemical Amperometry	[61]
Simoa (Single Molecule Array)	10^{-3}– ~10^{2}	Serum	0.013	4~5 h	100 μL	Digital fluorescence	[40]
NasRED	5×10^{-2}– 2×10^{6}	PBS Serum WB Synovial fluid	0.022 (in PBS)	20~25 min	6 μL	NasRED	This work

Table 2.

Values of the PED signals for TNF-α detection in spiked HPS samples in the presence of Adalimumab (10 nM, 100 nM) and ADA (10 nM, 100 nM). S_1: PED signal when Adalimumab was at 100 nM; S_2: PED signal when Adalimumab was at 10 nM. Signal difference: $\delta S = S_1 - S_2$.

	Low ADA (10 nM)			High ADA (100 nM)		
TNF-α concentration	**S_1**	**S_2**	**δS**	**S_1**	**S_2**	**δS**
50 nM	0.020	0.055	−0.035	0.067	0	0.067
5 nM	0.869	0.823	0.045	0.55	0.392	0.158
0.5 nM	1	0.935	0.064	0.783	0.541	0.241